PNAS RESEARCH ARTICLE | MEDICAL SCIENCES OPEN ACCESS

A ribavirin-induced ORF2 single-nucleotide variant produces defective hepatitis E virus particles with immune decoy function

Toni Luise Meister[a], Yannick Brüggemann[a], Maximilian K. Nocke[a], Rainer G. Ulrich[b,c], Jonas Schuhenn[d], Kathrin Sutter[d], André Gömer[a], Verian Bader[e,f], Konstanze F. Winklhofer[e,g], Ruth Broering[h], Lieven Verhoye[i], Philip Meuleman[i], Florian W. R. Vondran[j,k], Charline Camuzet[l], Laurence Cocquerel[l], Daniel Todt[a,m,1], and Eike Steinmann[a,n,1]

Edited by Xiang-Jin Meng, Virginia Polytechnic Institute and State University, Blacksburg, VA; received February 14, 2022; accepted June 23, 2022

Hepatitis E virus (HEV) is the causative agent of hepatitis E in humans and is the leading cause of enterically transmitted viral hepatitis worldwide. Ribavirin (RBV) is currently the only treatment option for many patients; however, cases of treatment failures or posttreatment relapses have been frequently reported. RBV therapy was shown to be associated with an increase in HEV genome heterogeneity and the emergence of distinct HEV variants. In this study, we analyzed the impact of eight patient-derived open reading frame 2 (ORF2) single-nucleotide variants (SNVs), which occurred under RBV treatment, on the replication cycle and pathogenesis of HEV. The parental HEV strain and seven ORF2 variants showed comparable levels of RNA replication in human hepatoma cells and primary human hepatocytes. However, a P79S ORF2 variant demonstrated reduced RNA copy numbers released in the supernatant and an impairment in the production of infectious particles. Biophysical and biochemical characterization revealed that this SNV caused defective, smaller HEV particles with a loss of infectiousness. Furthermore, the P79S variant displayed an altered subcellular distribution of the ORF2 protein and was able to interfere with antibody-mediated neutralization of HEV in a competition assay. In conclusion, an SNV in the HEV ORF2 could be identified that resulted in altered virus particles that were noninfectious in vitro and in vivo, but could potentially serve as immune decoys. These findings provide insights in understanding the biology of circulating HEV variants and may guide development of personalized antiviral strategies in the future.

hepatitis E virus | open reading frame 2 (ORF2) | viral variants | ribavirin | assembly

Significance

Hepatitis E virus (HEV) has increasing prevalence worldwide. However, little is known about the impact of single-nucleotide variants (SNV) on the replication cycle. Here, we report a ribavirin-induced open reading frame 2 (ORF2) SNV that demonstrats reduced RNA copies released in the supernatant and an impairment in the production of infectious particles. Furthermore, the P79S variant displays an altered subcellular distribution of the ORF2 protein and is able to impair antibody-mediated neutralization of HEV in a competition assay potentially acting as an immune decoy. These findings provide insights in understanding the biology of circulating HEV variants and may guide development of personalized antiviral strategies in the future.

Despite its rising global prevalence, hepatitis E is a disease that is mostly overlooked. Every year, more than 44,000 people die as a result of ∼20 million infections worldwide (1). Healthy individuals usually display no or only mild symptoms of viral hepatitis, such as fever, nausea, vomiting, and abdominal pain (2), while patients with preexisting liver disease, pregnant women, and immunocompromised individuals suffer from liver cirrhosis and liver failure (3). Pregnant women additionally present with increased mortality rates of >25% (4). Despite those liver-associated problems, there are also extrahepatic manifestations, such as hematopoietic disease, neurological disorders, and renal injury (5–9). The underlying agent, hepatitis E virus (HEV), is classed within the species of *Paslahevepirus balayani* (10), formerly known as *Orthohepevirus A*, which includes isolates from human, swine, wild boar, rat, and other mammals. HEV is a quasienveloped virus existing as both enveloped and non-enveloped particles (11, 12). To date, eight distinct genotypes (GT) of this species of the single-stranded RNA virus have been described (13), which display similar genomic structures. The positive orientated HEV genome is organized in three main open reading frames (ORF1 to ORF3) with a total length of 7.2 kb. Nonstructural proteins forming the HEV replicase complex, such as the RNA-dependent RNA polymerase (RdRp), RNA helicase, or methyltransferase, are encoded by ORF1, while the viral capsid protein is encoded by ORF2. During the HEV replication cycle, HEV produces at least three forms of ORF2 protein: infectious ORF2 (ORF2i), glycosylated ORF2 (ORF2g), and cleaved ORF2 (ORF2c) protein (14). The ORF2i protein is the structural component of infectious particles that is likely derived from the assembly of the intracellular ORF2 (ORF2intra) protein form. In contrast, ORF2g and ORF2c protein are not associated with infectious virions, but secreted in large amounts and are the most abundant antigens detected in patient sera (14). ORF3 encodes for a functional ion channel required for assembly and release of infectious particles by interacting with a variety of host factors (15).

In immunocompetent patients, acute hepatitis E usually does not involve antiviral therapy; however, chronically infected and immunocompromised patients often require

Author contributions: T.L.M., Y.B., L.C., D.T., and E.S. designed research; T.L.M., M.K.N., A.G., L.V., and C.C. performed research; R.G.U., J.S., K.S., K.F.W., R.B., P.M., and F.W.R.V. contributed new reagents/analytic tools; T.L.M., Y.B., M.K.N., A.G., V.B., D.T., and E.S. analyzed data; T.L.M. and E.S. wrote the paper; and T.L.M., Y.B., M.K.N., R.G.U., J.S., K.S., A.G., V.B., K.F.W., R.B., L.V., P.M., F.W.R.V., C.C., L.C., D.T., and E.S. reviewed and edited the original draft.

The authors declare no competing interest.

This article is a PNAS Direct Submission.

[1]To whom correspondence may be addressed. Email: daniel.todt@rub.de or eike.steinmann@rub.de.

This article contains supporting information online at http://www.pnas.org/lookup/suppl/doi:10.1073/pnas.2202653119/-/DCSupplemental.

Published August 15, 2022.

clinical intervention to clear the infection. Antiviral therapies include pegylated interferon (16–18), successfully implemented for many virus infections, and sofosbuvir (19, 20), a direct acting antiviral against hepatitis C virus, both of which have not yet been systematically evaluated in the context of HEV therapy. Recent studies have investigated the antiviral potential of silvestrol (21), zinc salts (22), and other possible drug candidates in vitro [reviewed in detail by Kinast et al. (23)], but the findings remain to be clinically validated. Lacking specific treatment options, the broad antiviral ribavirin (RBV) (24) is frequently used off-label. However, RBV therapy is often discontinued due to adverse side effects and is only effective in ∼80% of patients, implying that 20% of treated patients remain viremic (25). RBV treatment is specifically contraindicated in pregnant women and can give rise to variants such as G1634R, as well as other amino acid substitutions within the ORF1-encoded polyprotein, potentially contributing to treatment failure and poor clinical long-term outcomes (26–28). In this context, we recently identified viral populations of HEV harboring variations in the capsid-encoding ORF2 region during RBV therapy. With the use of an efficient HEV cell-culture model system, we characterized the impact of these ORF2 variants in the HEV replication cycle.

Results

RBV-Induced ORF2 Single-Nucleotide Variants Frequently Occur in HEV Patients. We recently observed the emergence of eight distinct amino acid substitutions within the ORF2 protein (P25S, G38S, A64T, G71R, P79S, S95P, V245I, and T324S) in HEV-infected individuals, that were associated with a sustained viral response despite RBV therapy (28). To determine if these single-nucleotide variants (SNVs) frequently occur in HEV-3 isolates, we analyzed 581 HEV-3 genomes that were annotated in the National Center for Biotechnology Information (NCBI) database for presence of the eight distinct ORF2 variants. All variants were found at varying frequencies between 1% and 39% of HEV patients (Fig. 1, green) and are classed within different GT3 subtypes. Sequences matching the consensus sequence (HEV-3 Kernow-C1/p6) occurred in 59 to 100% (Fig. 1, black). Of note, most HEV sequences deposited in the NCBI are mainly based on traditional Sanger sequencing and thus neglect minor variants in the HEV intrahost population. In summary, our recently observed HEV-3 amino acid substitutions have repeatedly occurred in infected individuals and thus likely represent viral variants with clinical implications for disease outcome and severity.

Production of Infectious HEV Particles Is Abrogated by ORF2 Variant P79S. To examine the influence of the identified ORF2 variants on the replication capacity of HEV, we introduced the different SNVs (P25S, G38S, A64T, G71R, P79S, S95P, V245I, and T324S) into the Kernow-C1/p6 strain (WT) (*SI Appendix*, Fig. S1*A*) and performed reverse-transcription quantitative polymerase chain reaction (RT-qPCR) to quantify viral RNA and immunofluorescence staining to detect ORF2 protein. Of note, the introduced mutations were not accompanied by changes in the ORF3 protein. In vitro-transcribed RNA of the eight ORF2 variants, WT, and a RdRp loss-of-function variant (GAA) were transfected into HepG2 cells and RNA was collected from cells and the supernatant at different time points. RNA copy numbers were determined by RT-qPCR using specific primers located within ORF2 but outside the mutated positions. The WT displayed constant RNA levels within cells and the supernatant over the observed timeframe

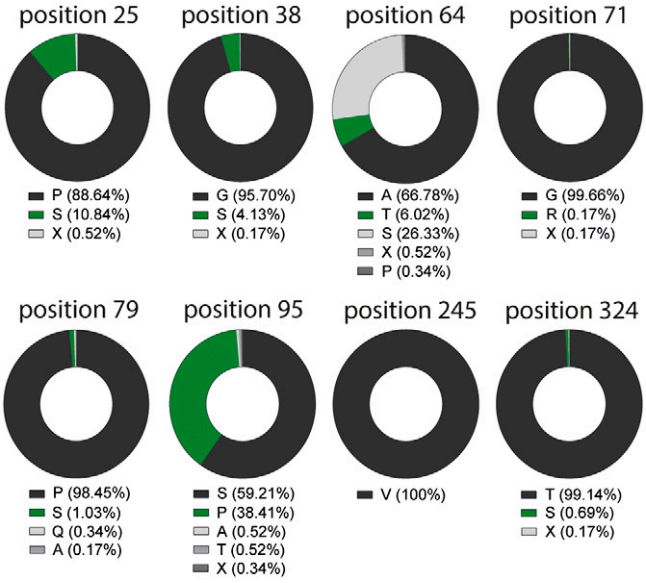

Fig. 1. Amino acid frequency of ORF2 variants at indicated sequence positions based on the NCBI database: 581 HEV-3 genomes were analyzed regarding the presence of the 8 distinct ORF2 variants. A matching amino acid composition with the consensus sequence of Kernow-C1/p6 is shown in black. Amino acid residues matching the ORF2 variant at those specific positions are depicted in green. Amino acids that neither match the consensus sequence of Kernow-C1/p6 nor the ORF2 variant at the positions 25, 38, 64, 71, 79, 95, 245, or 324 are colored in lighter shades of gray.

(Fig. 2*A*), while RNA levels for the replication-deficient variant GAA decreased over time (Fig. 2*B*).

Compared to WT, we further observed similar RNA levels within cells and supernatant for all ORF2 variants, except for P79S (Fig. 2 *C–J*). For P79S a reduction of RNA copy numbers was observed that occurred earlier and was more pronounced for RNA collected from the supernatant as compared to RNA collected from cells, indicating that the P79S amino acid substitution affects the release of viral progeny from the cell. To test whether the reduced RNA amount was associated with a reduction of ORF2 protein abundance, we performed immunofluorescence analysis to determine the number of ORF2 protein expressing cells following RNA transfection. Comparable numbers of HEV^+ cells for all ORF2 SNVs including the P79S variant were observed (*SI Appendix*, Fig. S1 *B* and *C*), implying that the P79S amino acid substitution potentially impairs productive virus assembly and release from an infected cell. Therefore, we examined the impact of the different ORF2 SNVs on the production of infectious viral particles using a recently described cell-culture system to generate high titers of infectious HEV (HEV_{CC}) (29, 30). To this end, in vitro-transcribed RNA was transfected into HepG2 cells and after 7 d non-enveloped and enveloped HEV_{CC} were harvested and used to infect HepG2/C3A cells (Fig. 3 *A–D*). Viral titers varied between 7.6×10^4 focus-forming units (FFU)/mL to 6.6×10^5 FFU/mL for non-enveloped HEV_{CC} (Fig. 3 *A* and *C*) and 6.8×10^1 FFU/mL to 8.6×10^2 FFU/mL for enveloped HEV_{CC} (Fig. 3 *B* and *D*). Overall, we observed comparable viral titers of non-enveloped particles for all ORF2 variants, except for P79S (Fig. 3 *A* and *C*). In case of the enveloped HEVcc variants, P25S, G38S, and G71R demonstrated 10-fold lower viral titers compared to WT with a complete loss of infectious virus progeny production for P79S (Fig. 3 *B* and *D*).

Similar results were obtained when inoculating primary human hepatocytes (PHHs) with non-enveloped HEV_{CC} ORF2 variants and subsequent evaluation of viral progeny

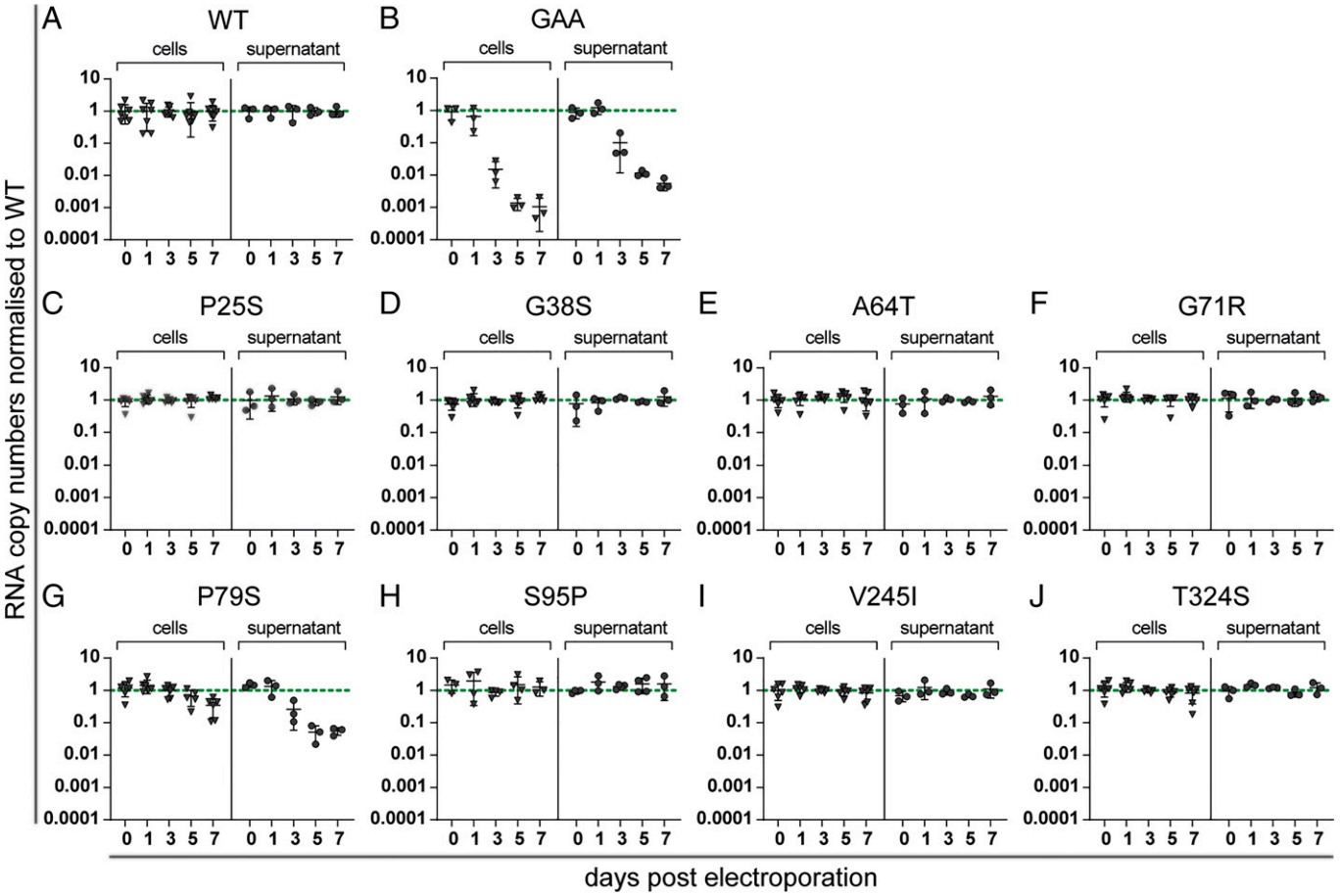

Fig. 2. HEV RNA replication and shedding of ORF2 variants into the supernatant at five different time points postelectroporation. (*A–J*) RNA copy numbers were determined by RT-qPCR and normalized to WT (dotted green line). Triangles represent the intracellular HEV RNA copies obtained from the cells (▼), while RNA copy numbers determined from the supernatant are depicted by circles (●). $n \geq 3 \pm$ SD.

production. RNA copy numbers within the cells (Fig. 3*E*) and the supernatant (Fig. 3*F*) were analyzed by RT-qPCR and the number of ORF2 protein-positive cells was determined by immunofluorescence staining (Fig. 3 *G* and *H*). As observed before, all ORF2 variants, except P79S, reached viral loads comparable to WT (Fig. 3 *E* and *F*). Within cells 1.5×10^6 to 7.0×10^6 HEV RNA copies/50 ng total RNA were detectable and between 1.5×10^6 to 3.5×10^6 HEV RNA copies/mL in the supernatant. In contrast, RNA copy numbers detectable for P79S were close to the lower limit of quantification (5.7×10^3 RNA copies/50 ng total RNA within the cells and 1.9×10^3 RNA copies/mL in the supernatant). Moreover, we did not observe ORF2 protein-positive cells as analyzed by immunofluorescence (Fig. 3*G*) for the P79S variant and the GAA control, while all other ORF2 variants showed similar numbers of ORF2 protein-positive cells (Fig. 3*H*). To test if the P79S variant also leads to a nonproductive infection in vivo, two human-liver chimeric mice were either inoculated with WT or P79S HEV_{CC}. In comparison to WT-infected mice, low to nondetectable RNA levels in the stool were observed for P79S inoculated mice (*SI Appendix*, Fig. S2) Overall, our results suggest comparable levels of replication and formation of infectious viral progeny for ORF2 variants, except for P79S, which displayed reduced levels of released RNA and abrogation of the production of infectious particles.

ORF2 Variant P79S Alters the Biophysical Properties of Enveloped HEV Particles. Amino acid exchanges within the viral capsid protein have been described to induce conformational changes causing deficiencies in virus particle assembly and release (31, 32). To analyze changes of biophysical properties based on sedimentation velocities, non-enveloped and enveloped HEV_{CC} were subjected to an iodixanol-step gradient ultracentrifugation (Fig. 4). Non-enveloped HEV has been reportedly enriched at higher densities (1.20 to 1.25 g/mL) as compared to enveloped virus, which peaks at lower densities (1.10 to 1.15 g/mL) (29, 33). In accordance, the majority of HEV RNA was detectable at 1.24 g/mL and 1.23 g/mL for non-enveloped WT (Fig. 4 *A*, *Upper*), and 1.09 g/mL and 1.06 g/mL for enveloped WT virions (Fig. 4 *A*, *Lower*). All other ORF2 variants showed comparable RNA distributions throughout the fractions for non-enveloped and enveloped particles, except for P79S. While the biophysical properties of non-enveloped P79S was similar to WT particles (Fig. 4 *G*, *Upper*), the majority of HEV RNA was detectable at higher densities for enveloped P79S virions (1.17 g/mL) (Fig. 4 *G*, *Lower*). These results indicate that the capsid protein produced by P79S is not being assembled or released like the WT HEV capsid protein.

ORF2 Variant P79S Generates Defective, Smaller HEV Particles. To further characterize the ORF2 alteration induced by the introduced amino acid substitution at position 79, ORF2 antigen abundance and the presence of different ORF2 protein isoforms was analyzed. First, the presence of ORF2 antigen following RNA transfection was analyzed by performing an antigen ELISA. In line with comparable percentages of ORF2 protein-positive cells (*SI Appendix*, Fig. S1), no significant differences between ORF2

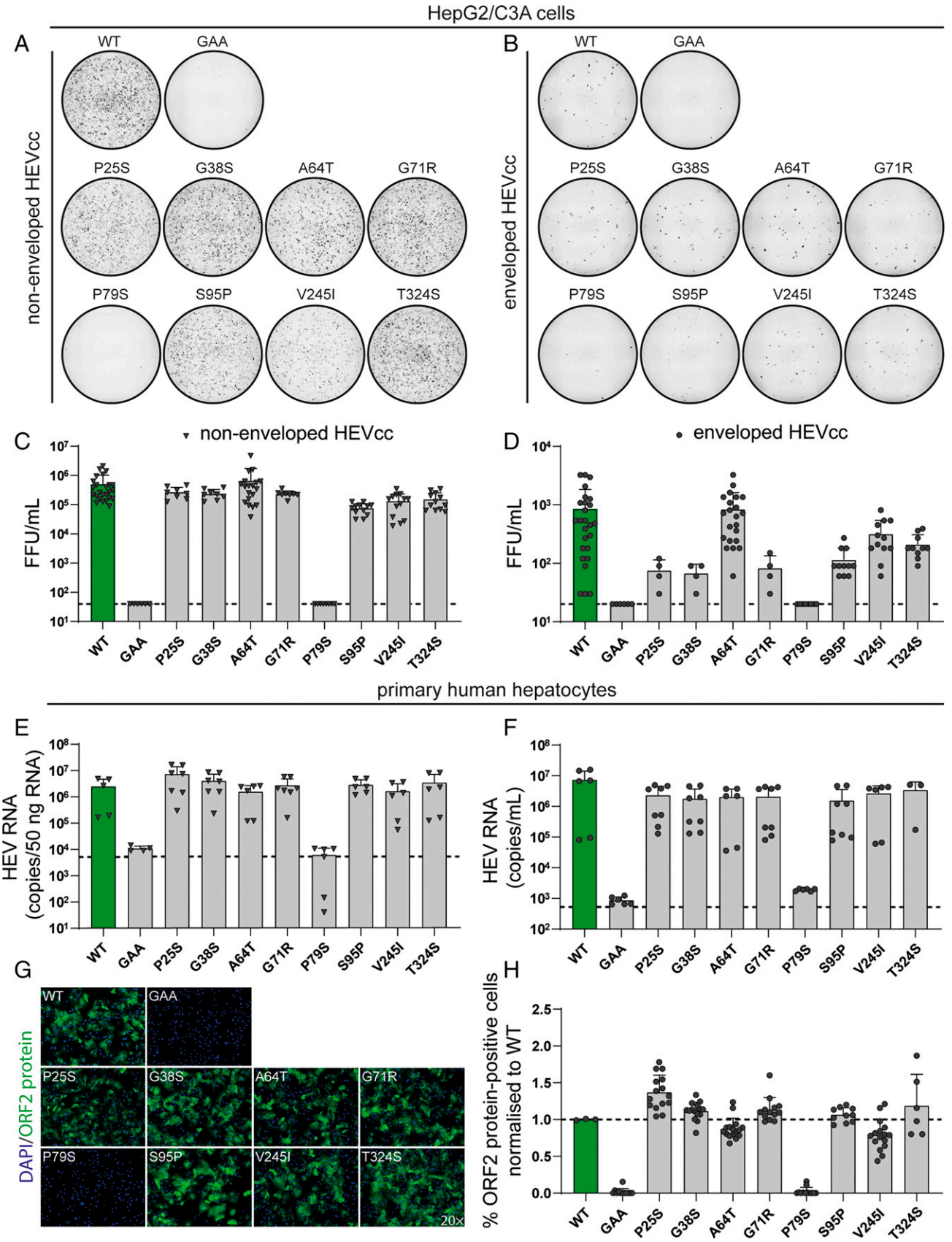

Fig. 3. Determination of production of infectious viral particles of ORF2 variants. Representative images of whole 96 wells of non-enveloped (*A*) or enveloped (*B*) HEVcc infected HepG2/C3A cells stained for ORF2 protein (black). Images were taken using a Keyence microscope with 4× magnification and processed using CellProfiler. Viral titers were determined by serial dilution of non-enveloped (*C*) and enveloped (*D*) HEV_{CC}. Dashed line indicates lower limit of quantification (LLOQ) (titers below LLOQ set to LLOQ); $n \geq 4 \pm$ SD. PHHs were infected with non-enveloped HEVcc (multiplicity of infection of 2) overnight and were incubated for 3 d. RNA was harvested from the cells (*E*) and the supernatant (*F*) to determine RNA copy numbers by RT-qPCR ($n \geq 3 \pm$ SD). (*G*) Representative fluorescence images of infected PHH stained for ORF2 protein. (*H*) The number of ORF2 protein-positive cells were determined by immunofluorescence staining using CellProfiler and normalized to WT ($n \geq 3 \pm$ SD). Dashed line indicates LLOQ.

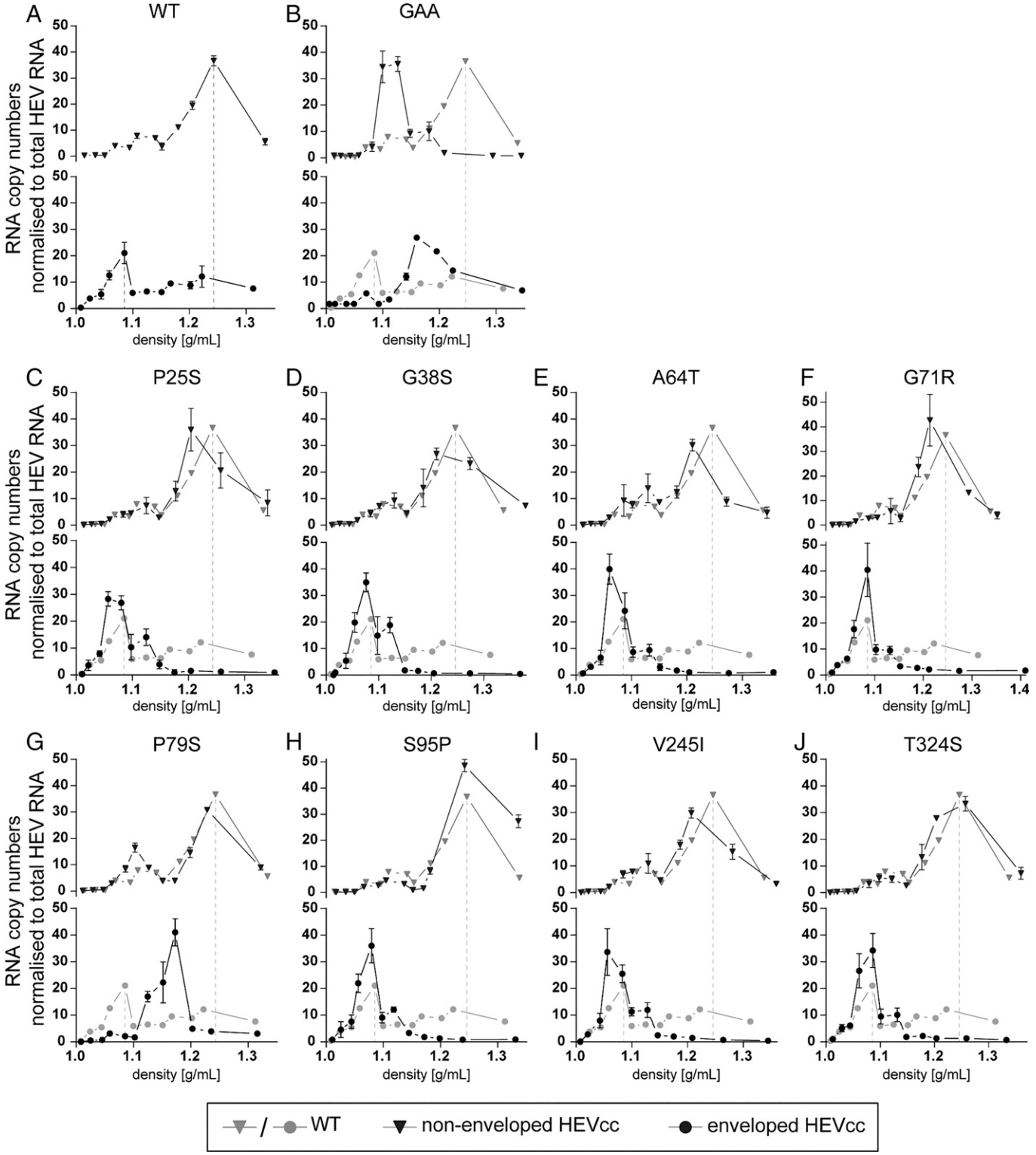

Fig. 4. Density gradient ultracentrifugation of non-enveloped and enveloped ORF2 variants with subsequent detection of HEV RNA. After ultracentrifugation the gradient was divided into twelve fractions. (*A–J*) Subsequently, density and RNA copy numbers were determined for each fraction by refractometry and RT-qPCR, respectively. Enveloped HEV_{CC} is represented as circles (●), while non-enveloped HEVcc is depicted as triangles (▼). The WT control (*A*) is included in every graph in gray (*B–J*).

protein levels associated with non-enveloped and enveloped WT and all ORF2 variants were detected, including P79S (Fig. 5 *A* and *B*). To analyze the effect of ORF2 variants on the production of different ORF2 protein isoforms, input Western blot and immunoprecipitations (IPs) of non-enveloped and enveloped HEV_{CC} using different monoclonal anti-ORF2 protein antibodies (P3H2, P1H1, and 4B2) with subsequent Western blot analysis were performed. Following IPs with P3H2, all ORF2 protein isoforms were detectable in all variants with the exception for GAA and reduced or absent signals for P79S (Fig. 5 *C* and *D*). P1H1, which recognizes only the infectious form of ORF2 protein (ORF2i) showed reduced and abrogated levels of intra- and extracellular ORF2 protein for P79S as compared to WT, respectively (Fig. 5 *E* and *F*). Finally,

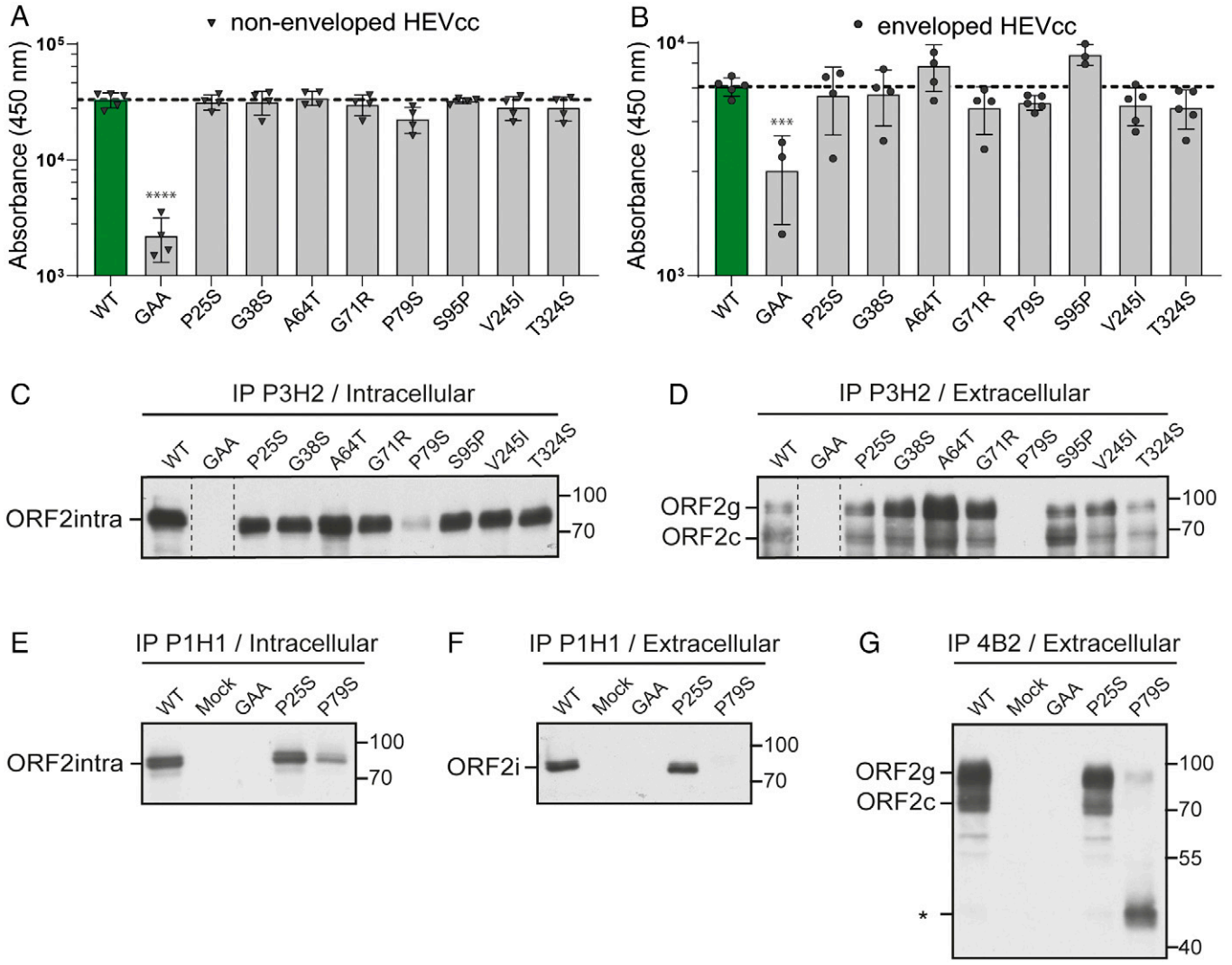

Fig. 5. Quantification and characterization of ORF2 antigen. Antigen ELISA (Wantai) to determine ORF2 antigen of non-enveloped (*A*, ▼) and enveloped HEV_{CC} (*B*, ●). For statistical analysis, a Dunnett's multiple comparisons test was applied using GraphPad Prism ($n \geq 3 \pm$ SD). (*C*–*G*) Coimmunoprecipitation with ORF2 protein specific antibodies (P3H2, P1H1, and 4B2) followed by Western blot analysis to distinguish between infectious (ORF2i), cleaved (ORF2c), and glycosylated (ORF2g) ORF2 protein isoforms of non-enveloped HEV_{CC} (*C* and *E*) and enveloped HEV_{CC} (*D*, *F*, and *G*). Protein signals were evaluated by chemiluminescence analysis using the monoclonal anti-ORF2 protein 1E6 antibody and a peroxidase-conjugated anti-mouse secondary antibody.

a conformation-dependent ORF2 protein antibody (4B2) (34) was used for IP, which showed again reduced and abrogated levels of ORF2g and ORF2c proteins for P79S, respectively. Additionally, a smaller ORF2 protein with a size of ∼45 kDa for P79S could be detected, which was absent for WT (Fig. 5*G*), as already observed in the input Western blots (*SI Appendix*, Fig. S3). To test if the assembly defect could be restored by WT ORF2 protein, HepG2/C3A cells expressing ORF2, as evidenced by immunofluorescence staining (HepG2/C3A_ORF2) (*SI Appendix*, Fig. S4*A*), were generated. HepG2/C3A_ORF2 were electroporated with RNA of either WT, P79S, or a replicon variant harboring a GFP within the ORF2 region to monitor *trans*-complementation efficiency (*SI Appendix*, Fig. S4*B*). The obtained non-enveloped HEV_{CC} were used to inoculate naïve HepG2/C3A cells and infected cells were detected by immunofluorescence staining using an ORF2 protein-specific antibody (*SI Appendix*, Fig. S4*C*). For WT, infected cells could be detected in HepG2/C3A_ORF2 and the respective control cells (HepG2/C3A_BLR), while infectious events for p6_GFP and P79S were only detected in HepG2/C3A_ORF2 cells (*SI Appendix*, Fig. S4*C*). Overall, our data suggest that the P79S variant confers an assembly defect and generates a smaller ORF2 protein, which can be *trans*-complemented by ectopic expression of WT ORF2.

Altered Subcellular Distribution of ORF2 Variant P79S. The assembly and budding site of HEV, as well as the mechanism of ORF2 protein oligomerization to form viral particles, are poorly understood (35). To examine whether P79S impairs virus assembly by altering ORF2 protein localization, the subcellular distribution of ORF2 protein was assessed by immunofluorescence staining following electroporation of WT and P79S in HepG2 cells over time (Fig. 6*A*). For WT the formation of distinct speckles 3 d post electroporation (dpe), was observed, whereas for the P79S variant the ORF2 protein remained evenly distributed throughout the cell over time (Fig. 6*A*). This phenomenon was further illustrated by displaying the distribution of fluorescence intensities (FI) 7 dpe in representative single cells (yellow boxes, Fig. 6 *B*–*E*) and by volumetric three-dimensional reconstitution of both ORF2 variants (Fig. 6*F* and Movies S1 and S2). We confirmed the same subcellular localization of ORF2 protein following infection of cells with

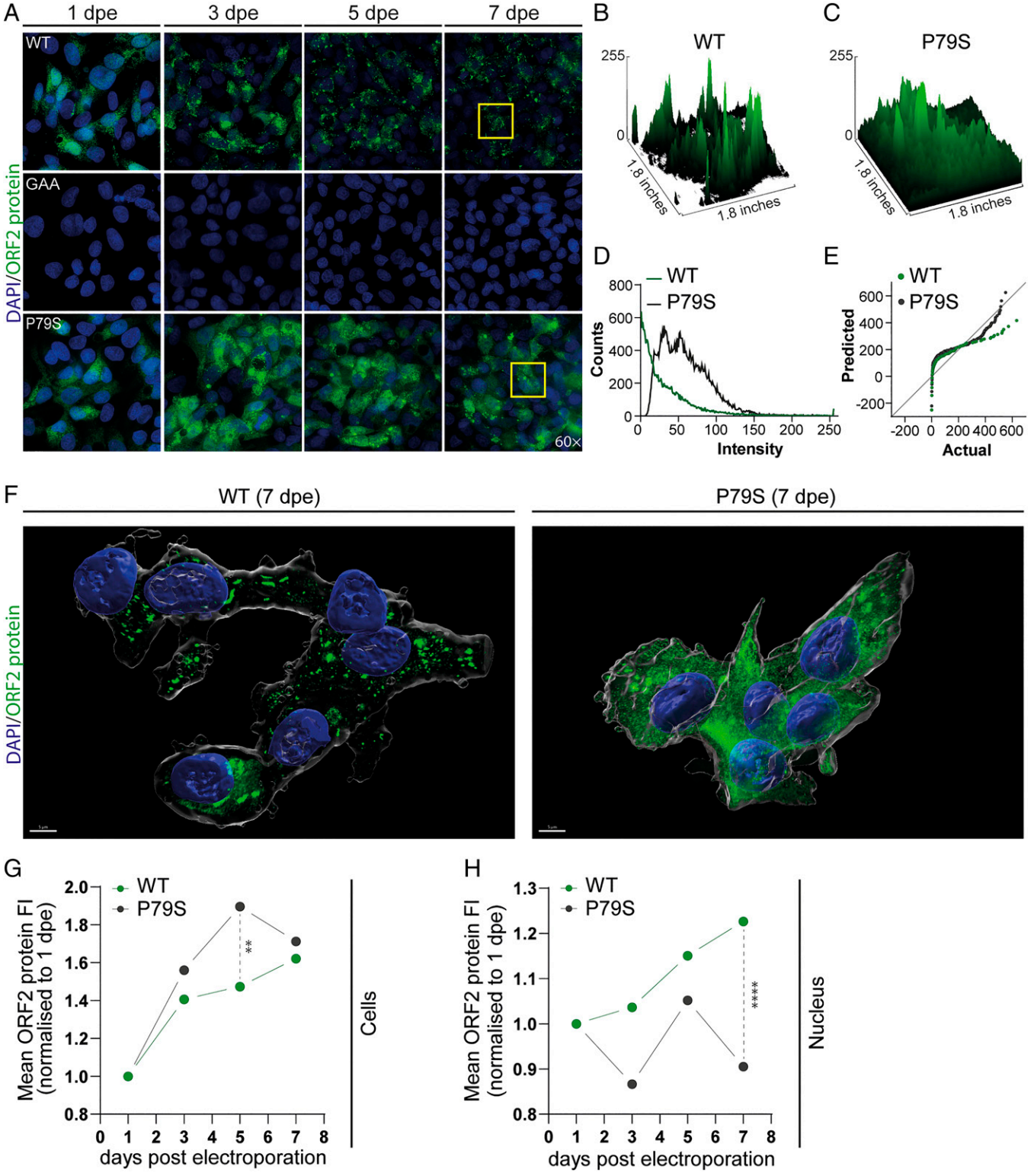

Fig. 6. Subcellular distribution for WT and P79S ORF2 protein in electroporated HepG2 cells. (*A*) Cells electroporated with in vitro-transcribed RNA of WT, GAA, and P79S were fixed and stained for ORF2 protein after 1, 3, 5, and 7 dpe. (*B* and *C*) Surface blot of the ORF2 protein fluorescence signal distribution of a single cell (yellow square in *A*). (*D* and *E*) Signal intensity of ORF2 protein for WT and P79S (yellow square in *A*). (*F*) Three-dimensional images of cells transfected with WT and P79S 7 dpe using structured illumination microscopy (SIM). Using CellProfiler, ORF2 protein-positive cells were encircled and the fluorescence intensity of ORF2 protein was determined. Mean ORF2 protein fluorescence intensity in the whole cell (*G*) and the nucleus (*H*) normalized to 1 dpe. (*G* and *H*) Statistical significance was determined using a one-way ANOVA with Šídák's multiple comparisons test.

WT HEV_{CC} to exclude potential differences between transfection and infection assays (*SI Appendix*, Fig. S5).

An absolute quantification of ORF2 protein in the whole cell revealed increased ORF2 expression over time for WT and only slightly lower ORF2 expression levels for the P79S variant 5 dpe, while comparable intensities for the remaining time points were measured (*SI Appendix*, Fig. S6 *A* and *B*). ORF2 protein has not only been described in the cytoplasm, but also to localize to the nucleus (36, 37). The quantified FI in the nuclear compartment increased with time for WT, in a

manner analogous to the whole-cell kinetics, but remained constant at a lower level within the nucleus for P79S (Fig. 6 *G* and *H* and *SI Appendix*, Fig. S6 *C* and *D*). Colocalization studies of the ORF2 WT and P79S variant with markers for mitochondria, Golgi apparatus, endoplasmic reticulum, early endosomes, lysosomes, or multivesicular bodies, demonstrated comparable signals between the ORF2 proteins and different cellular compartments (*SI Appendix*, Fig. S7). However, no codistribution was observed for either of the compartments and ORF2 protein. Next, we investigated the potential colocalization of ORF2 protein with double-stranded RNA (dsRNA), a replication intermediate. Using CellProfiler, ORF2 protein-positive cells were encircled to quantify the number of dsRNA speckles and analyze colocalization with the two ORF2 variants. Decreasing amounts of speckles for WT and P79S over time could be observed; however, for WT significantly more speckles were counted at 7 dpe (*SI Appendix*, Fig. S8 *A–D*). Additionally, for each encircled cell a Pearson's correlation coefficient was calculated and plotted over the course of time to investigate colocalization (*SI Appendix*, Fig. S8 *E–G*). Although no significant codistribution was observed, the highest Pearson's correlation coefficient for WT and P79S was observed 1 dpe, followed by a drop at 3 and 5 dpe.

Despite the accumulation of WT ORF2 protein in distinct areas, no colocalization was observed, but the amino acid exchange at position 79 resulted in an altered distribution with less concentrated ORF2 protein signals compared to the parental HEV, suggesting that virus assembly possibly relies on the accumulation of ORF2 protein.

P79S-Derived ORF2 Protein Remains Antigenic Toward Neutralizing Antibodies Reducing Antibody-Mediated Neutralization of WT HEV_{CC}. Since certain viruses secrete immune decoys in the form of antigens, such as receptors or noninfectious particles, we next tested if the P79S variant capsid protein is still antigenic and can compete for antibodies in the presence of WT. Therefore, naïve HepG2/C3A cells were infected with a fixed amount of non-enveloped WT HEV_{CC} and increasing volumes of P79S supernatant in the presence of anti-HEV serum (Fig. 7). Five days postinfection the cells were fixed and stained for ORF2 protein to determine the viral titers (Fig. 7*A*). Infection solely with WT resulted in viral titers of 400 FFU per well, while the addition of neutralizing antibodies led to a reduction to background levels (Fig. 7*B*). This neutralization effect of WT by the anti-HEV serum could be inhibited by a dose-dependent addition of the P79S variant in this competition assay. Viral titers of WT could be rescued to 35 FFU per well, indicating that the ORF2 variant P79S was able to bind neutralizing antibodies and inhibit antibody-mediated neutralization of WT.

Discussion

RBV therapy has been linked to a marked increase in viral genetic heterogeneity within all three ORFs of the HEV genome, potentially favoring the emergence of viral variants associated with treatment failure (28, 38). In this context, we recently observed the occurrence of various distinct amino acid substitutions within the capsid-encoding ORF2 region (28). Changes to the viral-encoded structural proteins can have a profound impact on the formation and properties of virions as currently observed for SARS-CoV-2 (i.e., altered binding affinities to target cells and antibodies favoring immune evasion) (39–41). Therefore, it is important to study and understand the HEV intrahost diversity and the emergence of distinct variants that occur during the

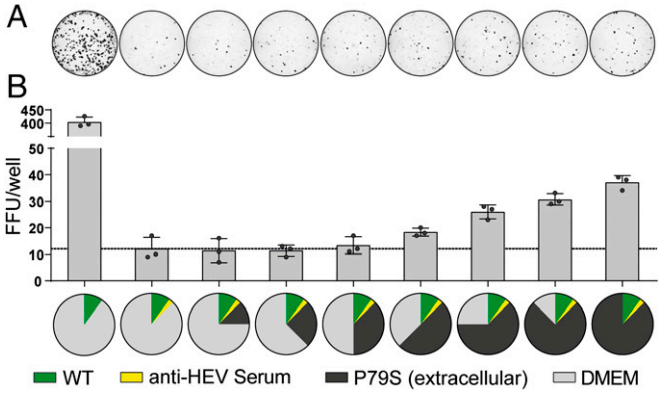

Fig. 7. Extracellular particles produced by P79S can compete for antibodies acting as immune decoys. HepG2/C3A cells were infected either solely with 1.25 parts non-enveloped WT or simultaneously with WT and increasing amounts of the extracellular form of P79S (1.25 to 8.75 parts). To each sample a defined volume of a human anti-HEV serum was added. The volume of each sample was set to 200 μL by adding DMEM. (*A*) Five days postinfection, the cells were stained for the presence of ORF2 protein (black). Images were taken using a Keyence microscope with 4× magnification and processed using CellProfiler. (*B*) FFUs were counted for each well and compared to the number of infected cells with the addition of anti-HEV serum. Dashed line indicates the number of FFU counted for the cells solely infected with WT and simultaneously treated with an anti-HEV serum.

course of viral infection. In the case of HEV, ORF2 mutations have been described to influence infectious particle formation by, for example, preventing dimer formation of ORF2 protein (42), or could theoretically influence immune evasion and treatment failure, as it has been shown for other viruses (43, 44). To examine the respective biological function of the identified capsid protein variants, we used a recently improved reverse-genetic HEV cell culture system that covers the complete viral replication cycle of HEV (29). The utilized system is based on the HEV-3 p6 strain, originally isolated by Shukla et al. (45) using fecal samples obtained from an HIV patient chronically coinfected with HEV. The virus was semipurified from the feces and used to inoculate several cell lines. Sequence analysis data showed an insertion of 58 amino acids of the human ribosomal subunit S17 (RSP17) into the hypervariable region of the ORF1 polyprotein, which was already present at low frequencies during the first passages and became the dominant variant in later passages (46). After six passages, an adapted virus was isolated and termed Kernow-C1/p6. In this study, we compared the biological functions of the ORF2 variants engineered into the Kernow-C1/p6 strain. Therefore, the genetic background of the analyzed HEV variants is not changed except for the indicated ORF2 alteration.

While seven ORF2 variants did not affect viral replication and infectivity, the P79S variant conferred a defect in virus assembly. In contrast to WT, this variant shed less RNA into the cell culture supernatant while replicating at similar rates over time (Fig. 2), and was unable to establish a productive infection in cell lines and PHHs (Fig. 3). *Trans*-complementation of P79S with WT ORF2 protein restored infectiousness, indicating the amino acid residue at position 79 is an essential determinant for infectious particle production (*SI Appendix*, Fig. S4). These results also indicate that assembly-defective variants could be rescued in infected hepatocytes in vivo to ensure viral dissemination. Additionally, density gradient ultracentrifugation showed a shift of secreted P79S toward higher densities (Fig. 4), implying altered virus particle formation. It was demonstrated that HEV produces several isoforms of the ORF2 protein with the ORF2i protein as the structural component of infectious particles (14, 47). The ORF2i and ORF2intra proteins are not glycosylated, while

ORF2g/c proteins are highly glycosylated and secreted, but are not associated with infectious virions. For the HEV variant, we observed that although similar amounts of ORF2 protein were produced by WT and P79S (Fig. 5*A* and *SI Appendix*, Fig. S1 *B* and *C*), decreased amounts of P79S ORF2g, and a lack of ORF2i and ORF2c isoforms compared to WT were detected by IP (Fig. 5 *C*–*F*).

In line with these findings, we observed reduced ORF2 protein FI within the nucleus of P79S transfected HepG2 cells compared to WT, although comparable ORF2 protein FIs were measured throughout the whole cell for both variants, suggesting that less P79S ORF2 protein was translocated into the nucleus (Fig. 6 *G* and *H* and *SI Appendix*, Fig. S6). ORF2 protein within the nucleus has already been described in liver biopsies of HEV-infected individuals (37). Recently, nuclear translocation of the ORF2 protein was shown to confer a fitness advantage to HEV, possibly related to suppression of the host immune response and an advantage in viral replication (36, 37, 48). Similarly, different patterns of ORF2 protein localization within the cytoplasm were observed. While P79S ORF2 protein remained evenly distributed throughout the cytoplasm, WT ORF2 protein accumulated in speckles of high intensity 3 to 7 dpe (Fig. 6 *A*–*F*). This was also the case for cells infected with non-enveloped WT, showing that ORF2 protein accumulation is not an artifact caused by electroporating cells with HEV RNA (*SI Appendix*, Fig. S5), but rather necessary to drive capsid assembly, which is disturbed when introducing the P79S amino acid substitution. ORF2 protein accumulation in distinct speckles has already been observed by others (48, 49) as so called viral factories (50, 51). This phenomenon has already been reported for other viruses and their structural proteins (52–56).

In addition to the accumulation of structural proteins, RNA replication frequently takes place in close proximity to these structures. RNA viruses, such as Zika virus, have been reported to reorganize microtubules and intermediate filaments (e.g., vimentin) to form virus-induced replication factories (57). These factories are sometimes surrounded by amorphous membranous material acting as scaffolds for virus replication and assembly, while they tend to exclude host proteins, as observed for the membranous web induced by HCV or dengue virus (58–60). In line with these findings, we observed partial codistribution of ORF2 protein with dsRNA, a replication intermediate of RNA viruses (*SI Appendix*, Fig. S8). Similarly, colocalization of ORF1 gene products with ORF2 and ORF3 proteins has been observed (50, 51), and it was recently described that HEV proteins and recycling compartment markers are codistributed in perinuclear structures found in ultrastructural analyses as a network of vesicular and tubular structures (50). These studies imply that HEV may also form viral factories, and the dynamic role of ORF2 protein during HEV replication and assembly needs to be further defined.

Extracellular enveloped P79S appeared to assemble a much smaller capsid protein compared to the WT strain (Fig. 5). How these smaller particles are generated (e.g., proteolytic degradation, premature translational termination) needs future investigation. For HEV, highly conserved hydrophobic regions were described to be involved in particle formation (61), building an icosahedral shell with 90 protrusions (62). However, truncated ORF2 protein has been shown to self-assemble and form empty virus-like particles (63, 64). These virus-like particles possessed antigenicity similar to authentic HEV particles, but were unable to produce infectious progeny (63). Such noninfectious particle secretion has been observed for many other viruses and can circumvent immunological clearance by the secretion of immune decoys in form of receptors (65–67) or empty capsids/envelopes (68, 69). For HEV, noninfectious particle secretion without encapsidated RNA has been recurrently described (14, 42, 47). We could show by a neutralizing competition assay that the secreted form of P79S could compete for neutralizing antibodies, thereby increasing infectious events for WT HEV (Fig. 7). Hence, the smaller ORF2 form produced by P79S could possibly be part of an immune evasion strategy evolved by HEV potentially acting as an immune decoy to circumvent immunological clearance.

In conclusion, an SNV of HEV ORF2 could be identified that generates assembly-defective particles leading to nonproductive infection. This ORF2 variant could be rescued *in trans* and lead to an antibody-mediated impairment of HEV neutralization, supporting an immune decoy function as evolutionary advantage. These results reveal a previously unrecognized aspect in HEV biology and shed new light on the immune evasion mechanisms and pathogenesis of this virus.

Materials and Methods

Cell Culture. Human liver cell line HepG2 (ATCC Nr.: HB-8065) was cultured in Dulbeco's Modified Eagle's Medium (DMEM, supplemented with 10% [vol/vol] fetal calf serum [FCS], 1% [vol/vol] nonessential amino acids [NEAA], 100 IU/mL penicillin, 100 μg/mL streptomycin, and 2 mM L-glutamine). For infection experiments, an HepG2 subclone (HepG2/C3A) was utilized displaying greater infection efficiencies cultured in Eagle's minimum essential medium (MEM, supplemented with 10% [vol/vol] ultralow IgG FCS [Gibco, Cat. no. 16250-078, Lot 1939770], 2 mM L-glutamine, 100 μg/mL gentamicin, 1 mM sodium pyruvate, and 1% [vol/vol] NEAAs). HepG2 and HepG2/C3A cells were further grown on rat collagen-coated (SERVA Electrophoresis) cell-culture dishes. PHHs were prepared from nontumorous tissue obtained from freshly resected livers, as previously described (70, 71). All patients provided written documentation of their informed consent. The study conformed to the ethical guidelines of the 1975 Declaration of Helsinki and was approved by the Institutional Review Board (Ethics Committee) of the medical faculty at the University Duisburg-Essen. Human biological samples were provided by the Westdeutsche Biobank Essen (WBE, University Hospital Essen, University of Duisburg-Essen, Essen, Germany; approval 18-WBE-048). PHHs were seeded into collagen I-coated culture plates or coverslips and cultured in William's E medium (supplemented with 5% [vol/vol)]FCS, 1% [vol/vol] NEAA, 100 IU/mL penicillin, 100 μg/mL streptomycin, 2 mM GlutaMAX, 2% [vol/vol] dimethyl sulfoxide, 10 mM Hepes, 2.5 μg/mL hydrocortisone, 55 ng/mL epidermal growth factor, and 5 μg/mL insulin). PLC3 cells, a subclone of PLC/PRF/5 hepatoma cells (14), were cultured as previously described (36). All cells were kept at 37 °C in a 5% (vol/vol) CO_2 incubator.

Data Availability. All study data are included in the main text and *SI Appendix*.

ACKNOWLEDGMENTS. We thank Martina Friesland and Patrick Behrendt for providing the HepG2/C3A_BLR and HepG2/C3A_ORF2 cells; all members of the Department for Molecular and Medical Virology for helpful suggestions and discussions; and the Westdeutsche Biobank Essen (University Hospital Essen, University of Duisburg-Essen, Essen, Germany; approval WBE reference no. 20-WBE-102) for providing human biological samples. R.G.U. acknowledges funding by the German Centre for Infection Diseases (DZIF, TTU "Emerging Infections": TTU 01.808_00). K.S. was supported by a grant from the German Research Foundation (DFG) (Grant SU1030-2-1). K.F.W. is supported by the DFG (FOR 2848 and Germany's Excellence Strategy, EXC 2033-390677874 RESOLV). Confocal laser-scanning and superresolution-structured illumination microscopy were funded by the DFG and the State Government of North Rhine-Westphalia (INST 213/840-1 FUGG). L.C. was supported by the French agency Agence Nationale de Recherches sur le SIDA-Maladies infectieuses émergentes, Pasteur Institute of Lille, Région Hauts-de-France, and Inserm-transfert. D.T. was supported by a grant from the DFG (Project no. 448974291) and by the German Federal Ministry of Education and Research (BMBF) (project: VirBio, grant number: 01KI2106). E.S. was supported by the German Federal Ministry of Health (ZMVI1-2518FSB705), by the DFG (398066876/GRK 2485/1), and by a grant of the DZIF (TTU 05.823).

Author affiliations: [a]Department for Molecular and Medical Virology, Ruhr University Bochum, Bochum, 44801 Germany; [b]Institute of Novel and Emerging Infectious Disease, Friedrich-Loeffler-Institut, 17493 Greifswald-Insel Riems, Germany; [c]German Centre for Infection Research, Partner site Hamburg-Lübeck-Borstel-Riems, 17493 Greifswald-Insel Riems, Germany; [d]University Hospital Essen, Institute for Virology, University Duisburg-Essen, 47057 Essen, Germany; [e]Department of Molecular Cell Biology, Institute of Biochemistry and Pathobiochemistry, Ruhr University Bochum, Bochum, 44801 Germany; [f]Department of Biochemistry of Neurodegenerative Diseases, Institute of Biochemistry and Pathobiochemistry, Ruhr University Bochum, Bochum, 44801 Germany; [g]Cluster of Excellence RESOLV, 44801 Bochum, Germany; [h]Department of Gastroenterology, Hepatology, and Transplant Medicine, University Hospital Essen, University Duisburg-Essen, 47057 Essen, Germany; [i]Faculty of Medicine and Health Sciences, Department of Diagnostic Sciences, Laboratory of Liver Infectious Diseases, Ghent University, B-9000 Ghent, Belgium; [j]Department of General, Visceral, and Transplant Surgery, Hannover Medical School, 30625 Hannover, Germany; [k]German Centre for Infection Research, Partner site Hannover-Braunschweig, 30625 Hannover, Germany; [l]Pasteur Institute of Lille, Centre Hospitalier Universitaire Lille, CNRS, INSERM, University of Lille, U1019-UMR 9017-Center for Infection and Immunity of Lille, 59000 Lille, France; [m]European Virus Bioinformatics Center, 07743 Jena, Germany; and [n]German Centre for Infection Research, External Partner Site, 44801 Bochum, Germany

1. World Health Organization, Hepatitis E: Fact sheet (2021). https://www.who.int/news-room/fact-sheets/detail/hepatitis-e. Accessed 1 August 2022.
2. A. N. Desai, Hepatitis E. *JAMA* **323**, 1862 (2020).
3. N. Kamar, H. R. Dalton, F. Abravanel, J. Izopet, Hepatitis E virus infection. *Clin. Microbiol. Rev.* **27**, 116–138 (2014).
4. M. S. Khuroo, S. Kamili, Aetiology, clinical course and outcome of sporadic acute viral hepatitis in pregnancy. *J. Viral Hepat.* **10**, 61–69 (2003).
5. S. Pischke, P. Behrendt, M. P. Manns, H. Wedemeyer, HEV-associated cryoglobulinaemia and extrahepatic manifestations of hepatitis E. *Lancet Infect. Dis.* **14**, 678–679 (2014).
6. P. Colson *et al.*, Severe thrombocytopenia associated with acute hepatitis E virus infection. *J. Clin. Microbiol.* **46**, 2450–2452 (2008).
7. P. Mishra, M. Mahapatra, R. Kumar, H. P. Pati, Autoimmune hemolytic anemia and erythroid hypoplasia associated with hepatitis E. *Indian J. Gastroenterol.* **26**, 195–196 (2007).
8. A. Sood, V. Midha, N. Sood, Guillain-Barré syndrome with acute hepatitis E. *Am. J. Gastroenterol.* **95**, 3667–3668 (2000).
9. F. S. Fousekis, I. V. Mitselos, D. K. Christodoulou, Extrahepatic manifestations of hepatitis E virus: An overview. *Clin. Mol. Hepatol.* **26**, 16–23 (2020).
10. M. A. Purdy *et al.*, ICTV virus taxonomy profile: Hepeviridae 2022 (2022). https://talk.ictvonline.org/ictv-reports/ictv_online_report/positive-sense-rna-viruses/w/hepeviridae. Accessed 10 June 2022.
11. X. Yin, C. Ambardekar, Y. Lu, Z. Feng, Distinct entry mechanisms for nonen and quasi-enveloped hepatitis E viruses. *J. Virol.* **90**, 4232–4242 (2016).
12. S. Chapuy-Regaud *et al.*, Characterization of the lipid envelope of exosome encapsulated HEV particles protected from the immune response. *Biochimie* **141**, 70–79 (2017).
13. D. B. Smith *et al.*, Proposed reference sequences for hepatitis E virus subtypes. *J. Gen. Virol.* **97**, 537–542 (2016).
14. C. Montpellier *et al.*, Hepatitis E virus lifecycle and identification of 3 forms of the ORF2 capsid protein. *Gastroenterology* **154**, 211–223.e8 (2018).
15. Q. Ding *et al.*, Hepatitis E virus ORF3 is a functional ion channel required for release of infectious particles. *Proc. Natl. Acad. Sci. U.S.A.* **114**, 1147–1152 (2017).
16. N. Kamar *et al.*, Three-month pegylated interferon-alpha-2a therapy for chronic hepatitis E virus infection in a haemodialysis patient. *Nephrol. Dial. Transplant.* **25**, 2792–2795 (2010).
17. L. Alric, D. Bonnet, G. Laurent, N. Kamar, J. Izopet, Chronic hepatitis E virus infection: Successful virologic response to pegylated interferon-alpha therapy. *Ann. Intern. Med.* **153**, 135–136 (2010).
18. E. B. Haagsma, A. Riezebos-Brilman, A. P. van den Berg, R. J. Porte, H. G. Niesters, Treatment of chronic hepatitis E in liver transplant recipients with pegylated interferon alpha-2b. *Liver Transpl.* **16**, 474–477 (2010).
19. V. L. Dao Thi *et al.*, Sofosbuvir inhibits hepatitis E virus replication in vitro and results in an additive effect when combined with ribavirin. *Gastroenterology* **150**, 82–85.e4 (2016).
20. M. van der Valk, H. L. Zaaijer, A. P. Kater, J. Schinkel, Sofosbuvir shows antiviral activity in a patient with chronic hepatitis E virus infection. *J. Hepatol.* **66**, 242–243 (2017).
21. D. Todt *et al.*, The natural compound silvestrol inhibits hepatitis E virus (HEV) replication in vitro and in vivo. *Antiviral Res.* **157**, 151–158 (2018).
22. N. Kaushik *et al.*, Zinc salts block hepatitis E virus replication by inhibiting the activity of viral RNA-dependent RNA polymerase. *J. Virol.* **91**, e00754-17 (2017).
23. V. Kinast, T. L. Burkard, D. Todt, E. Steinmann, Hepatitis E virus drug development. *Viruses* **11**, 485 (2019).
24. N. Kamar *et al.*, Treatment of HEV infection in patients with a solid-organ transplant and chronic hepatitis. *Viruses* **8**, 222 (2016).
25. European Association for the Study of the Liver, EASL clinical practice guidelines on hepatitis E virus infection. *J. Hepatol.* **68**, 1256–1271 (2018).
26. Y. Debing *et al.*, A mutation in the hepatitis E virus RNA polymerase promotes its replication and associates with ribavirin treatment failure in organ transplant recipients. *Gastroenterology* **147**, 1008–11.e7; quiz e15-6 (2014).
27. Y. Debing *et al.*, Hepatitis E virus mutations associated with ribavirin treatment failure result in altered viral fitness and ribavirin sensitivity. *J. Hepatol.* **65**, 499–508 (2016).
28. D. Todt *et al.*, In vivo evidence for ribavirin-induced mutagenesis of the hepatitis E virus genome. *Gut* **65**, 1733–1743 (2016).
29. D. Todt *et al.*, Robust hepatitis E virus infection and transcriptional response in human hepatocytes. *Proc. Natl. Acad. Sci. U.S.A.* **117**, 1731–1741 (2020).
30. T. L. Meister, M. Klöhn, E. Steinmann, D. Todt, A cell culture model for producing high titer hepatitis E virus stocks. *J. Vis. Exp.* (160), e61373 (2020).
31. R. Yang *et al.*, Papillomavirus capsid mutation to escape dendritic cell-dependent innate immunity in cervical cancer. *J. Virol.* **79**, 6741–6750 (2005).
32. M. D. Lauver *et al.*, Antibody escape by polyomavirus capsid mutation facilitates neurovirulence. *eLife* **9**, e61056 (2020).
33. P. Behrendt *et al.*, Hepatitis E virus (HEV) ORF2 antigen levels differentiate between acute and chronic HEV infection. *J. Infect. Dis.* **214**, 361–368 (2016).
34. M. A. Riddell, F. Li, D. A. Anderson, Identification of immunodominant and conformational epitopes in the capsid protein of hepatitis E virus by using monoclonal antibodies. *J. Virol.* **74**, 8011–8017 (2000).
35. X. Ju, Q. Ding, Hepatitis E virus assembly and release. *Viruses* **11**, 539 (2019).
36. M. Ankavay *et al.*, New insights into the ORF2 capsid protein, a key player of the hepatitis E virus lifecycle. *Sci. Rep.* **9**, 6243 (2019).
37. D. Lenggenhager *et al.*, Visualization of hepatitis E virus RNA and proteins in the human liver. *J. Hepatol.* **67**, 471–479 (2017).
38. D. Todt, T. L. Meister, E. Steinmann, Hepatitis E virus treatment and ribavirin therapy: Viral mechanisms of nonresponse. *Curr. Opin. Virol.* **32**, 80–87 (2018).
39. B. Korber *et al.*; Sheffield COVID-19 Genomics Group, Tracking changes in SARS-CoV-2 spike: Evidence that D614G increases infectivity of the COVID-19 virus. *Cell* **182**, 812–827.e19 (2020).
40. E. C. Thomson *et al.*; ISARIC4C Investigators; COVID-19 Genomics UK (COG-UK) Consortium, Circulating SARS-CoV-2 spike N439K variants maintain fitness while evading antibody-mediated immunity. *Cell* **184**, 1171–1187.e20 (2021).
41. D. Planas *et al.*, Reduced sensitivity of SARS-CoV-2 variant Delta to antibody neutralization. *Nature* **596**, 276–280 (2021).
42. J. Graff *et al.*, Mutations within potential glycosylation sites in the capsid protein of hepatitis E virus prevent the formation of infectious virus particles. *J. Virol.* **82**, 1185–1194 (2008).
43. A. Ciurea *et al.*, Viral persistence in vivo through selection of neutralizing antibody-escape variants. *Proc. Natl. Acad. Sci. U.S.A.* **97**, 2749–2754 (2000).
44. G. E. Price, R. Ou, H. Jiang, L. Huang, D. Moskophidis, Viral escape by selection of cytotoxic T cell-resistant variants in influenza A virus pneumonia. *J. Exp. Med.* **191**, 1853–1867 (2000).
45. P. Shukla *et al.*, Cross-species infections of cultured cells by hepatitis E virus and discovery of an infectious virus-host recombinant. *Proc. Natl. Acad. Sci. U.S.A.* **108**, 2438–2443 (2011).
46. P. Shukla *et al.*, Adaptation of a genotype 3 hepatitis E virus to efficient growth in cell culture depends on an inserted human gene segment acquired by recombination. *J. Virol.* **86**, 5697–5707 (2012).
47. X. Yin *et al.*, Origin, antigenicity, and function of a secreted form of ORF2 in hepatitis E virus infection. *Proc. Natl. Acad. Sci. U.S.A.* **115**, 4773–4778 (2018).
48. K. Hervouet *et al.*, An arginine-rich motif in the ORF2 capsid protein regulates the hepatitis E virus lifecycle and interactions with the host cell. *bioRxiv* [Preprint] (2021). https://www.biorxiv.org/content/10.1101/2021.05.26.445820v2. Accessed 1 August 2022.
49. R. Johne *et al.*, An ORF1-rearranged hepatitis E virus derived from a chronically infected patient efficiently replicates in cell culture. *J. Viral Hepat.* **21**, 447–456 (2014).
50. C. Bentaleb *et al.*, The endocytic recycling compartment serves as a viral factory for hepatitis E virus. *bioRxiv* [Preprint] (2021). https://www.biorxiv.org/content/10.1101/2021.10.14.464345v1. Accessed 1 August 2022.
51. K. Metzger *et al.*, Processing and subcellular localization of the Hepatitis E virus replicase: Identification of candidate viral factories. *Front. Microbiol.***13**, 1664-302X (2022).
52. T. C. Hobman *et al.*, Assembly of rubella virus structural proteins into virus-like particles in transfected cells. *Virology* **202**, 574–585 (1994).
53. S. Thomas *et al.*, Chikungunya virus capsid protein contains nuclear import and export signals. *Virol. J.* **10**, 269 (2013).
54. Z. Shang, H. Song, Y. Shi, J. Qi, G. F. Gao, Crystal structure of the capsid protein from Zika virus. *J. Mol. Biol.* **430**, 948–962 (2018).
55. M. Gabriel *et al.*, Dengue virus capsid protein dynamics reveals spatially heterogeneous motion in live-infected-cells. *Sci. Rep.* **10**, 8751 (2020).
56. Y. Miyanari *et al.*, The lipid droplet is an important organelle for hepatitis C virus production. *Nat. Cell Biol.* **9**, 1089–1097 (2007).
57. M. Cortese *et al.*, Ultrastructural characterization of Zika virus replication factories. *Cell Rep.* **18**, 2113–2123 (2017).
58. C. J. Neufeldt *et al.*, The hepatitis C virus-induced membranous web and associated nuclear transport machinery limit access of pattern recognition receptors to viral replication sites. *PLoS Pathog.* **12**, e1005428 (2016).
59. N. L. Meyers, K. A. Fontaine, G. R. Kumar, M. Ott, Entangled in a membranous web: ER and lipid droplet reorganization during hepatitis C virus infection. *Curr. Opin. Cell Biol.* **41**, 117–124 (2016).
60. L. Chatel-Chaix, R. Bartenschlager, Dengue virus- and hepatitis C virus-induced replication and assembly compartments: The enemy inside–Caught in the web. *J. Virol.* **88**, 5907–5911 (2014).
61. S.-W. Li *et al.*, Mutational analysis of essential interactions involved in the assembly of hepatitis E virus capsid. *J. Biol. Chem.* **280**, 3400–3406 (2005).
62. B. V. Prasad, D. O. Matson, A. W. Smith, Three-dimensional structure of calicivirus. *J. Mol. Biol.* **240**, 256–264 (1994).
63. T. C. Li *et al.*, Expression and self-assembly of empty virus-like particles of hepatitis E virus. *J. Virol.* **71**, 7207–7213 (1997).
64. T. S. Y. Guu *et al.*, Structure of the hepatitis E virus-like particle suggests mechanisms for virus assembly and receptor binding. *Proc. Natl. Acad. Sci. U.S.A.* **106**, 12992–12997 (2009).
65. E. K. Hoebe *et al.*, Epstein-Barr virus-encoded BARF1 protein is a decoy receptor for macrophage colony stimulating factor and interferes with macrophage differentiation and activation. *Viral Immunol.* **25**, 461–470 (2012).
66. D. Wang, W. Bresnahan, T. Shenk, Human cytomegalovirus encodes a highly specific RANTES decoy receptor. *Proc. Natl. Acad. Sci. U.S.A.* **101**, 16642–16647 (2004).
67. A. Bukreyev *et al.*, The secreted form of respiratory syncytial virus G glycoprotein helps the virus evade antibody-mediated restriction of replication by acting as an antigen decoy and through effects on Fc receptor-bearing leukocytes. *J. Virol.* **82**, 12191–12204 (2008).
68. G. E. Rydell, K. Prakash, H. Norder, M. Lindh, Hepatitis B surface antigen on subviral particles reduces the neutralizing effect of anti-HBs antibodies on hepatitis B viral particles in vitro. *Virology* **509**, 67–70 (2017).
69. K. L. Shingler *et al.*, The enterovirus 71 procapsid binds neutralizing antibodies and rescues virus infection in vitro. *J. Virol.* **89**, 1900–1908 (2015).
70. M. Werner *et al.*, All-in-one: Advanced preparation of human parenchymal and non-parenchymal liver cells. *PLoS One* **10**, e0138655 (2015).
71. M. Kleine *et al.*, Explanted diseased livers–A possible source of metabolic competent primary human hepatocytes. *PLoS One* **9**, e101386 (2014).